Phase detection through four-wave mixing in an optical fiber

Amira S. Ahsan[a,*] **Aneesh Sobhanan**[b] **Deepa Venkitesh**[b] **and Govind P. Agrawal**[a]

[a]University of Rochester, The Institute of Optics, Rochester, New York, United States
[b]Indian Institute of Technology Madras, Department of Electrical Engineering, Madras, Chennai, India

Abstract. A scheme for detecting the phase of an incoming optical signal is systematically optimized and demonstrated experimentally. It makes use of four-wave mixing in a highly nonlinear fiber but differs from a phase-sensitive amplifier by its focus on phase detection, rather than on phase-dependent noise reduction. This experimental setup combines the signal with its phase-conjugated idler at the same frequency, before sending the combination to a photodetector. Experimental results show that the ratio of maximum and minimum currents can exceed 1000 even at a relatively low pump power of 10 mW. The proposed scheme may be useful for detecting the signal phase in coherent communication systems without the need of heterodyne detection. © *2020 Society of Photo-Optical Instrumentation Engineers (SPIE)* [DOI: 10.1117/1.OE.59.11.116109]

Keywords: optics; phase detection; four-wave mixing; nonlinear optics.

Paper 20201065 received Sep. 14, 2020; accepted for publication Nov. 6, 2020; published online Nov. 26, 2020.

1 Introduction

The nonlinear process of four-wave mixing (FWM) in optical fibers has been studied extensively because of its multitude of applications.[1] Among other applications, it can be used for realizing parametric amplifiers and frequency converters. Some applications make use of the phase-conjugate nature of the idler wave generated. Indeed, phase conjugation has been used in recent years for improving the performance of optical communication systems[2,3] and for reducing the amplifier-added noise through the technique of phase-sensitive amplification.[4–6] A technique based on parametric amplification was proposed in Ref. 7 to demultiplex a quadrature phase-shift keying (PSK) signal to the binary PSK format. Furthermore, applications of the phase-sensitive parametric processing are not restricted to the optical communication domain. It forms the underlying basis of enhanced phase measurement sensitivity using nonlinear interferometers[8] and in quantum metrology applications.[9]

In this work, we ask whether FWM-induced phase conjugation can be used to detect the phase of an incoming signal. This idea is related to a 1996 study[10] where the use of phase conjugation was proposed to replace the use of a local oscillator in a coherent telecommunication receiver. Here, we employ a different experimental setup to show that phase detection with high sensitivity is indeed possible in a system where the signal and idler waves oscillating at the same frequency are incident on a photodetector. Their interference creates a current whose magnitude at any time depends on the signal phase at that time. Similar demonstrations on phase-sensitive amplification were presented emphasizing its amplification and the phase regeneration properties,[6,11–13] a single-ended parametric coherent receiver was proposed in Ref. 14, however without systematic optimization in-terms of the input power ratio. In this paper, we present the systematic characterization and optimization of a system capable of measuring the phase of an optical signal. We demonstrate both experimentally and numerically that with the proper optimization of the power ratio with which the signal and idler mix, the ratio of maximum and minimum currents

*Address all correspondence to Amira S. Ahsan, aahsan@ur.rochester.edu

can exceed 1000 even at a relatively low pump power of 10 mW. Numerical simulations based on the nonlinear Schrödinger equation [1] agree with our measurements. We also discuss how the proposed technique can be applied for detecting the signal phase in coherent communication systems without employing heterodyne detection.

2 Principle of Operation

Figure 1 shows two schemes that can be employed for phase detection. The first scheme employs a dual-pump configuration of FWM in which the frequency ω_s of the input signal lies exactly in the middle of the frequencies ω_{p1} and ω_{p2} associated with the two pumps. This is similar to the configuration used usually for the demonstration of two-level phase quantization.[15] Its main advantage is that the idler wave is generated at the frequency of the signal ω_s, as seen from the energy conservation requiring $\omega_i = \omega_{p1} + \omega_{p2} - \omega_s$. Furthermore, the parametric gain responsible for the growth of the idler depends on the relative phase difference of the three interacting waves.[16]

In the second scheme shown in Fig. 1, a single pump at frequency ω_p is launched into a highly nonlinear fiber (HNLF), together with a control signal (C) at the frequency ω_c, and the actual signal (S) at frequency $\omega_s = 2\omega_p - \omega_c$. The idler generated through the FWM of the pump and the control C in this situation coincides with the frequency of the signal S whose phase needs to be detected. Similar to scheme 1, the amplification of the signal and the growth of the idler depends on the relative phase between the mixing waves. The use of control C for FWM allows us to control the idler's amplitude and phase in our experiments.

We first discuss a simplified model of the phase-detection process. For both schemes shown in Fig. 1, we filter the spectral contents centered at the frequency ω_i of the idler wave. Since the signal is also present at the same frequency, the two optical fields interfere at a photodetector placed after the optical filter. As a result, the current generated at the detector can be written as

$$I(\phi_s) = R_d \left| \sqrt{P_s^{\text{out}}} e^{i\phi_s} + \sqrt{P_i^{\text{out}}} e^{i\phi_i} \right|^2, \tag{1}$$

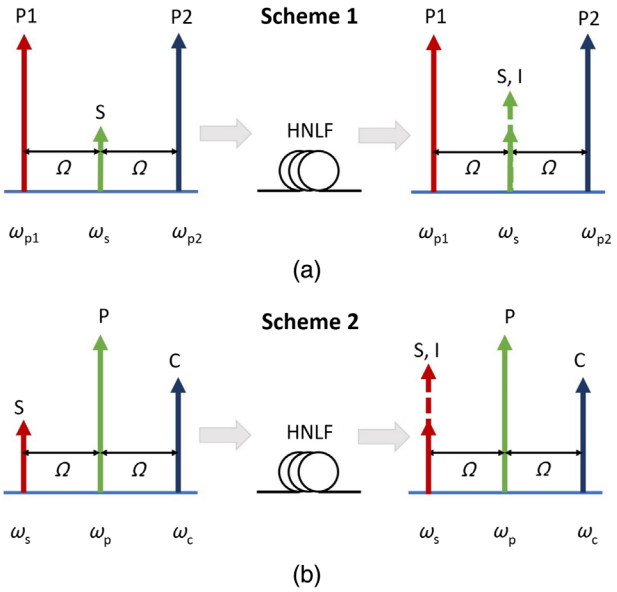

Fig. 1 Schematic illustration of two FWM schemes in the spectral domain using an HNLF. In the dual-pump scheme (a) P1 and P2 denote the frequency of the two pumps and the signal frequency lies in the middle. (b) In the second scheme, the pump frequency lies in the middle of the waves represented by C and S. The frequency of the idler coincides with that of the signal S whose phase needs to be detected.

where R_d is the responsivity of the detector, P_s^{out} and P_i^{out} represent the signal and idler powers at the fiber's output, and ϕ_s and ϕ_i represent their phase, respectively.

In the FWM process under scheme 1, the idler phase ϕ_i is related to the phase of the signal ϕ_s as $\phi_i = 2\bar{\phi}_p - \phi_s$, where $\bar{\phi}_p = (\phi_{p1} + \phi_{p2})/2$ is the average phase of the two pumps. In the case of scheme 2, $\bar{\phi}_p$ represents the phase of the single pump. When the phase of the control C is the same as that of the signal S, we can write the detector current in the form

$$I(\phi_s) = R_d\left[P_s^{\text{out}} + P_i^{\text{out}} + 2\sqrt{P_s^{\text{out}}P_i^{\text{out}}}\cos(2(\phi_s - \bar{\phi}_p))\right]. \tag{2}$$

This result shows how the detector current depends on the signal phase and thus can be used to deduce its value. The current becomes maximum and minimum for two values of ϕ_s differing by 90° and oscillates with a period π. However, if we set the input phase of C such that $\phi_c = \phi_p$, the idler phase becomes $\phi_i = \phi_p$ in Eq. (2) and we obtain

$$I(\phi_s) = R_d\left[P_s^{\text{out}} + P_i^{\text{out}} + 2\sqrt{P_s^{\text{out}}P_i^{\text{out}}}\cos(\phi_s - \bar{\phi}_p)\right]. \tag{3}$$

In this case, the current oscillates with a period 2π. This feature is desirable for practical applications of Scheme 2.

The quality of phase-to-intensity conversion can be quantified through a maximum-minimum ratio (MMR) of these two detector currents, defined as

$$\text{MMR} = \frac{I_{\max}}{I_{\min}} = \left(\frac{\sqrt{P_s^{\text{out}}} + \sqrt{P_i^{\text{out}}}}{\sqrt{P_s^{\text{out}}} - \sqrt{P_i^{\text{out}}}}\right)^2. \tag{4}$$

A large MMR indicates that two-phase values close to each other can be easily distinguished. As the formula in Eq. (3) relating the output current to the signal's phase is not linear, a true measure of phase sensitivity would be the derivative $dI/d\phi_s$.

We note that MMR is related to the concept of the gain-extinction ratio used in the context of phase-sensitive amplifiers. In the ideal situation, it becomes infinite when the signal and idler powers are equal at the output of the fiber. In practice, it becomes large (but never infinite) because of the dark current, thermal noise, and shot noise of the receivers. Incoming optical signal itself may be noisy because of the phase noise of lasers and spontaneous emission added by optical amplifiers. It is noteworthy that MMR includes the effects of all these sources of noise. Also, it is often not practical to equalize the power levels for the signal and idler fields at the output of the fiber. Thus, a measurement of MMR can be used to judge the effectiveness of the proposed scheme.

3 Numerical Simulations

To estimate the values of the MMR in a practical situation, we use numerical simulations using the parameters appropriate for the experiments discussed later. For this purpose, we solve the nonlinear Schrödinger equation numerically. This equation is given as[1]

$$\frac{\partial A}{\partial z} + i\frac{\beta_2}{2}\frac{\partial^2 A}{\partial t^2} = i\gamma|A|^2 A, \tag{5}$$

where β_2 is the group-velocity dispersion (GVD) parameter and γ is the nonlinear parameter of the HNLF used in our experiment. Our 1-km-long HNLF has $\gamma = 11.1\ \text{W}^{-1}/\text{km}$ and a GVD parameter of $\beta_2 = 0.75\ \text{ps}/(\text{nm-km})$ at wavelengths near 1550 nm. In this fiber, since the GVD parameter is positive for all the waves participating in the FWM process, complete phase matching is not possible since the sign of the phase mismatch due to dispersion and that due to nonlinearity are both positive. The efficiency of the FWM process is thus reduced. As a result, even though an idler wave is generated, its power at the output of the fiber remains relatively small and

the signal is also not amplified (no modulation instability). In other words, the pumped fiber is not operating as a parametric amplifier, even though its output remains phase-sensitive.

In the case of scheme 1, we solve Eq. (5) with the input

$$A(0,t) = \sqrt{P_s}e^{i\phi_s} + \sqrt{P_{p1}}e^{-i\Omega t}e^{i\phi_{p1}} + \sqrt{P_{p2}}e^{i\Omega t}e^{i\phi_{p2}}, \tag{6}$$

where P_{p1}, P_{p2}, and P_s are the input powers of the two pumps and the signal, respectively, and $\Omega = \omega_s - \omega_{p1}$ the pump-signal frequency difference. The pump and signal phase are included as ϕ_{p1}, ϕ_{p2}, and ϕ_s, respectively. In the case of scheme 2, the input takes the form

$$A(0,t) = \sqrt{P_p}e^{i\phi_p} + \sqrt{P_c}e^{i\Omega t}e^{i\phi_c} + \sqrt{P_s}e^{-i\Omega t}e^{i\phi_s}. \tag{7}$$

In this case, the signal-pump frequency shift is defined as $\Omega = \omega_c - \omega_p$. All other variables have the same meaning as for the scheme 1. The use of Eq. (5) with three input fields is more accurate than solving four coupled equations corresponding to the four waves participating in the FWM process, as this approach includes the effects of self-phase modulation, cross-phase modulation, and FWM automatically and captures the effects of cascaded FWM.

In the case of scheme 1, the signal frequency, $\nu_s = \omega_s/2\pi$, corresponds to a wavelength of 1550.11 nm and the frequencies of the two pumps are $\nu_s \pm 20$ GHz. While solving Eq. (5), we maintain a constant signal power and increase the total pump power from 9 (8 mW) to 22 dBm (160 mW), divided equally between the two pumps. Figure 2 shows how the calculated MMR varies with the pump power for input signal powers of $P_s = -6$ dBm (circles) and -14 dBm (squares). It is evident that MMR does not vary much with changes in the signal power at a constant pump power. In contrast, it changes drastically with changes in pump power, reaching a maximum value of about 30 dB at a total pump power of 19 dBm ($P_{p1} = P_{p2} = 40$ mW). A further increase in pump power results in a decreasing MMR. We attribute this decrease to the nonlinear phase introduced at high pump powers.

The curves with diamond and triangle symbols in Fig. 2 show how the calculated MMR varies with pump power under scheme 2 for $P_c = 5$ and -6 dBm, respectively. We use the following procedure to find the optimum launch power for the signal. We initially set $P_s = 0$ in Eq. (7) and launch only the pump and control signal waves into the fiber. By solving Eq. (5), we find the output power P_i^{out} of the idler wave. We choose the input power of the signal S equal to this value and vary the phase. Then, we solve Eq. (5) again and determine the MMR value shown in Fig. 2. It is clear that the scheme 2 provides much larger values of the MMR at a given pump power. Moreover, a peak value of 40 dB can be realized at a modest pump power of

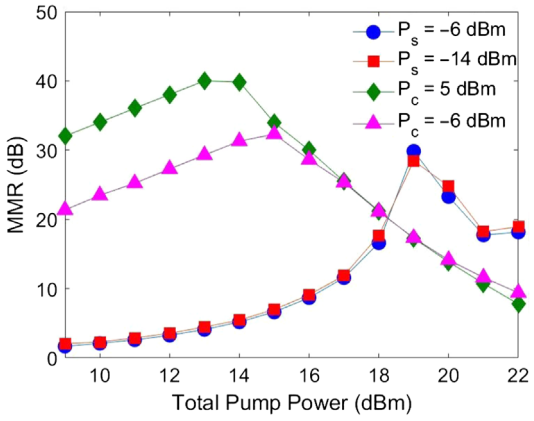

Fig. 2 Numerically calculated values of the MMR as a function of total pump power for the two schemes shown in Fig. 1. Curves with blue circles and red squares are for scheme 1 at signal power of -6 and -14 dBm, respectively. The curve with green diamonds is for scheme 2 at a constant C power of 5 dBm. The input power of S was optimized at every pump power as explained in the text. Similarly, for a constant C power of -6 dBm, the curve with the pink triangles is obtained.

about 13 dBm (20 mW) and control signal power of 5 dBm. Numerical simulations clearly indicate that the second scheme is superior to the first one. Furthermore, the second scheme offers an addition degree of freedom as it allows us to control the relative phase of the output at the S frequency, as discussed in the experimental section. For these reasons, we have chosen the scheme 2 for our experiments. It is noted that at lower pump power levels, the conversion efficiency is relatively smaller. The denominator of Eq. (4), in an ideal case should be zero, and hence, MMR should not be influenced by the magnitude of the numerator. However, in a practical scenario, the denominator is limited by the noise floor of the measurement device. In our simulations, we have intentionally added noise to mimic the noise floor observed in the experiments. Hence, when the input power increases, the numerator increases (for a constant denominator), and hence the MMR increases. In scheme 2, for a given power of C and fixed detuning, the idler (I) which gets generated at the signal frequency is determined by the pump power. We obtain the best MMR by varying the signal power accordingly as described in the optimization method earlier. So at lower pump power, due to the lower idler efficiency, the MMR is also lower. At high pump power, the nonlinear phase mismatch and presence of higher harmonics play the major role in reduction of MMR.[12]

4 Experiment Results and Discussion

Figure 3 shows the experimental setup used to demonstrate the feasibility of phase detection using the scheme 2 of Fig. 1. To ensure the frequency and phase synchronization of three input waves, they are generated using a phase modulator (PM). The 1550.11-nm output of a continuous-wave, narrow-line-width semiconductor laser is passed through a polarization controller (PC) before it enters the PM. When a 20-GHz microwave signal is applied, the PM creates a frequency comb around the input optical frequency, The comb line at 1550.11 nm is designated as the pump, and the comb lines shifted by ± 20 GHz are selected as the C and S signals (see scheme 2 in Fig. 1). The three optical fields are passed through a wave shaper, which allows us to manipulate their power levels. The initial relative phase difference among the three waves is also controlled by the wave shaper so that the phases of C and S are correlated. As all comb lines are phase coherent at the comb generation stage, this correlation can be realized in practice.

The output of the wave-shaper is amplified by an erbium-doped fiber amplifier followed by an optical filter used to reduce the amplified emission noise (ASE). Total input power to the fiber at any wavelength is restricted to below 13 dBm to avoid stimulated Brillouin scattering.[1] To filter out any back-scattered light, a circulator is used between the ASE filter and the 1-km long HNLF used for the experiment. An optical spectrum analyzer (OSA) is used to monitor the output of the HNLF.

In Fig. 4(a), we show the experimentally observed spectra for one specific input power levels of $P_p = 9.4$ dBm, $P_c = 4.7$ dBm, and $P_s = -15.3$ dBm. Both the control and actual signal have the same phase. For comparison, we show the numerically simulated spectrum in Fig. 4(b) under the identical operating conditions. In both cases, the red and blue curves correspond to the maximum and minimum amplitudes of the idler, as the relative signal phase, $\Delta\phi_s = \phi_s - \bar{\phi}_p$ is varied. The numerical spectral lines are much sharper compared to the experimental ones because we presumed here the phase noise of the pump, and signal waves are neglected.

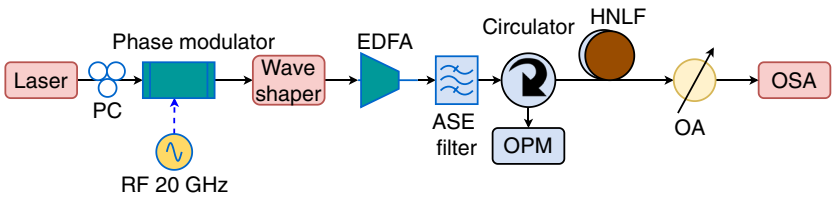

Fig. 3 Experimental setup used for the second FWM scheme in Fig. 1. PC, polarization controller; RF, radio frequency; PM, phase modulator; WS, wave shaper; OPM, optical power meter; ASE, amplified emission noise; HNLF, highly nonlinear fiber; OA, optical attenuator; OSA, optical spectrum analyzer.

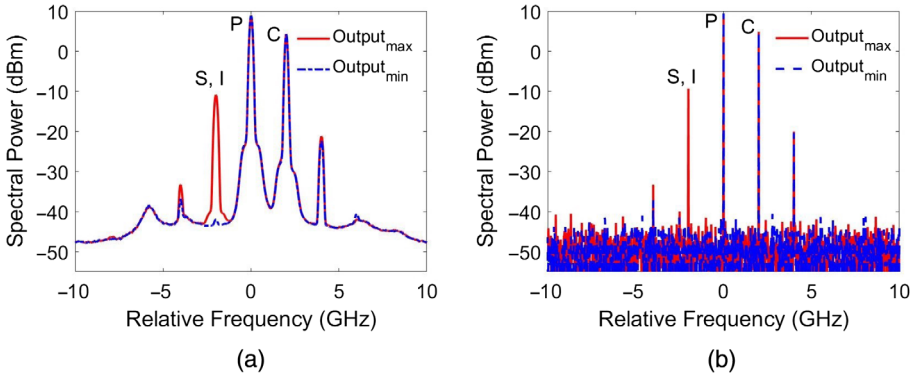

Fig. 4 (a) Observed output spectra for input powers of $P_P = 9.4$ dBm, $P_C = 4.7$ dBm, and $P_s = -15.3$ dBm with zero relative phase between C and S. The red and blue lines represent the output spectra when MMR is maximized or minimized. (b) Numerically simulated spectra in these two input conditions

However, the amplitudes of all spectral lines are in reasonable agreement. We have added the ASE noise in the simulation to match with the experimental noise floor. The additional sidebands generated through cascaded FWM were observed experimentally as also predicted numerically.

Periodic variations of the power at the detector are shown in Fig. 5 for two values of the control phase by sweeping the relative signal phase from 0 to 2.5π (red dots). In Fig. 5(a), the control and signal phases are the same, while in Fig. 5(b), the phase of control is equal to the pump phase. For comparison, we also show the numerically predicted values (blue curves) in the two cases. The numerical and experimental curves exhibit good agreement over a dynamic range exceeding 30 dB. In Fig. 5(a), the oscillation period is π, as expected from Eq. (1). An MMR of about 31 dB is obtained experimentally, which is in excellent agreement with the predicted value of 32.6 dB. In Fig. 5(b), the oscillation period is 2π, as shown in Eq. (3),[16] while the MMR remains nearly unchanged. It is noteworthy that the accuracy of measured MMR is limited by the noise floor to some extent.

We also studied the dependence of the MMR on the ratio P_p/P_c of the pump and control powers at the input end. The blue dots in Fig. 6 show the theory predictions at a constant pump power of $P_P = 9.4$ dBm while varying P_c. In each case, the signal power is found numerically by solving the nonlinear Schrodinger equation with $P_s = 0$ and then setting P_s equal to the calculated idler power. As seen from the straight line in Fig. 6, MMR is reduced linearly as P_c decreases. This feature is related to the reduced idler power generated through FWM for smaller control powers. The MMR values measured in two different experiments are shown in Fig. 6 and agree reasonably well with the numerical predictions.

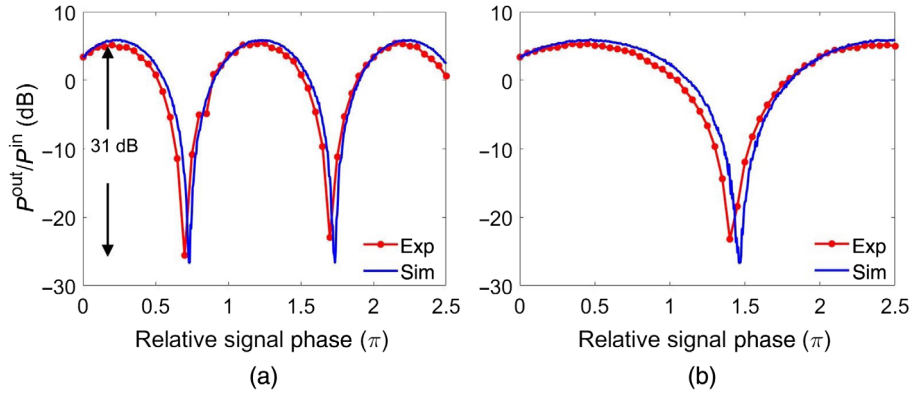

Fig. 5 (a) Power ratio of the filtered output at the idler frequency as a function of relative signal phase $\Delta\phi_s$. Simulated curve is also shown for comparison. (b) Observed power ratio when the phase of control was identical to the pump phase.

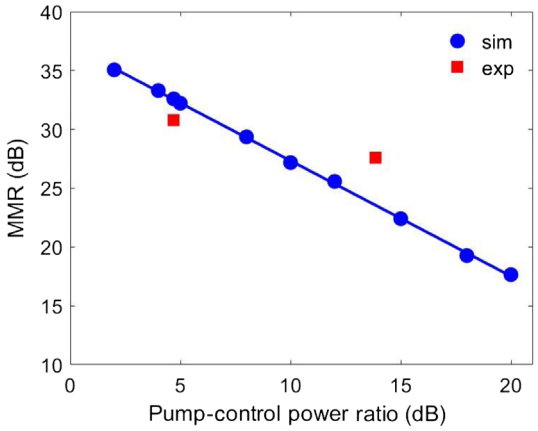

Fig. 6 MMR versus the pump-control signal power ratio. A constant pump power of 9.4 dBm is maintained, while the control signal power is varied. For each value of C input power, the S input power value is determined as explained earlier. The blue circles represent the numerical results. The line of best fit is shown in blue. Experimentally observed values are shown by the red squares.

One may wonder how the phase synchronization between C and S can be realized for telecommunication applications where two independent lasers will be used for these two signals. One possible solution is to employ injection locking of a local laser by injecting the incoming signal S, whose output can be used for C. The pump can be selected from an optical frequency comb (based on the frequency of the incoming signal S), which in turn could be injection locked by S, thus satisfying the requirement of phase correlation between S and the pump. Scheme 2 enables unique identification of phase values of range π. Phase discrimination in the full 2π range is possible by making measurements on both quadratures of the detector current with the help of a 90° hybrid (a device used for coherent systems). A slope-detection technique can also be used for this purpose. All-optical compensation of chromatic dispersion through mid-span spectral inversion, without the need of digital signal processing (DSP), has already been demonstrated.[2,3] The polarization diversity in scheme 2 can be addressed using orthogonally polarized degenerate pump.

5 Conclusions

A novel technique for detecting the phase of an incoming optical signal is proposed and demonstrated experimentally. It makes use of FWM inside an HNLF but differs from a phase-sensitive amplifier by its focus on phase detection. We discuss two schemes that combine the signal with its phase-conjugated idler at the same frequency, before sending the combination to a photodetector. We use numerically simulations for judging the relative merits of the two schemes and choose the one that allows phase detection in a wider range. Experimental results show that the ratio of maximum and minimum powers (MMR) at the detector can exceed 1000 even at a relatively low pump power of 10 mW. Different values of pump to signal ratio were used for optimization and to realize the highest MMR in the experiments. An MMR of 31 dB was achieved experimentally and this values agrees well with the predicted value of 32.6 dB. The required pump power was modest (< 11 dBm) and was below the threshold of stimulated Brillouin scattering for the 1-km-long HNLF used in the experiment. The proposed technique requires only direct detection for measuring the phase of an incoming signal. The scheme is a generalized technique to optimize the MMR of the system irrespective of the input signal power. Based on the input signal power the optimized values can differ. The idea here is to emphasize the importance of systematic optimization so that acceptable MMR is achievable with low energy consumption. We also analyze and prove the effectiveness of scheme 2 over scheme 1. The phase-detection technique described in this paper paves a way for potentially avoiding the need for coherent detection and subsequent DSP.

Acknowledgments

National Science Foundation (Grant No. ECCS-1933328); Department of Science and Technology, Government of India; SPARC, Ministry of Human Resources Development, Government of India; Visvesvaraya PhD Scheme- MEITY-PHD-2695, Ministry of Electronics and Information Technology, Govt of India. The authors declare no conflicts of interest.

References

1. G. P. Agrawal, *Nonlinear Fiber Optics*, 6th ed., Academic Press (2019).
2. M. A. Z. Al-Khateeb et al., "Experimental demonstration of 72% reach enhancement of 3.6 Tbps optical transmission system using mid-link optical phase conjugation," *Opt. Express* **26**, 23960–23968 (2018).
3. A. Sobhanan et al., "Dispersion and nonlinearity distortion compensation of the QPSK/16QAM signals using optical phase conjugation in nonlinear SOAs," *IEEE Photonics Technol. Lett.* **12**, 1–7 (2020).
4. M. Gao et al., "Evolution of the gain extinction ratio in dual-pump phase sensitive amplification," *Opt. Lett.* **37**, 1439–1441 (2012)
5. M. Karlsson, "Transmission systems with low noise phase-sensitive parametric amplifiers," *J. Lightwaves Technol.* **34**, 1411–1423 (2015).
6. P. A. Andrekson and M. Karlsson, "Fiber-based phase-sensitive optical amplifiers and their applications," *Adv. Opt. Photonics* **12**, 367–428 (2020).
7. A. Lorences-Riesgo et al., "Quadrature demultiplexing using a degenerate vector parametric amplifier," *Opt. Express* **22**, 29424–29434 (2014).
8. Z. Y. Ou, "Enhancement of the phase-measurement sensitivity beyond the standard quantum limit by a nonlinear interferometer," *Phys. Rev. A* **85**, 023815, 2012.
9. F. Hudelist et al., "Quantum metrology with parametric amplifier-based photon correlation interferometers," *Nat. Commun.* **5**, 3049, 2014.
10. G. P. Agrawal, "Phase detection in optical communication systems through phase conjugation," *Quantum Semiclass. Opt.* **8**, 383–385 (1996).
11. A. Agarwal et al., "Optical filter optimization using phase-sensitive amplification with unequalized signal/idler inputs," in *CLEO*, pp. 1–2 (2016).
12. A. Lorences-Riesgo et al., "Experimental analysis of degenerate vector phase-sensitive amplification," *Opt. Express* **22**, 21889–21902, 2014.
13. R. Slavík et al., "All-optical phase and amplitude regenerator for next-generation telecommunications systems," *Nat. Photonics* **4**, 690–695, 2010.
14. A. Kumpera et al., "Parametric coherent receiver," *Opt. Express* **23**, 12952–12964 (2015).
15. M. Gao et al., "Efficient phase regeneration of DPSK signal by sideband-assisted dual-pump phase-sensitive amplifier," *Electron. Lett.* **49**, 140–141 (2013).
16. R. Tang et al., "Gain characteristics of a frequency nondegenerate phase-sensitive fiber-optic parametric amplifier with phase self-stabilized input," *Opt. Express* **13**, 10483–10493 (2005).

Amira S. Ahsan received her BS degree in electrical and computer engineering from Lafayette College in 2013. She is a PhD student at the University of Rochester Institute of Optics in Rochester, New York, USA, studying nonlinear phenomena in graded-index fibers.

Aneesh Sobhanan received his Bachelor of Technology degree in electronics and communication engineering from the College of Engineering Attingal, Cochin University of Science and Technology, Kerala, India in 2009. He received his Master of Technology degree in electrical engineering from the Indian Institute of Technology Madras, Chennai, India, in 2014. He is currently a PhD student at the Department of Electrical Engineering, Indian Institute of Technology Madras, Chennai, India. His research interests include applications of nonlinear optics, optical signal processing for communication systems.

Deepa Venkitesh received her PhD in physics in 2009 from the Indian Institute of Technology Bombay, Mumbai, India. She is currently a professor at the Department of Electrical Engineering, Indian Institute of Technology Madras, Chennai, India. Her research interests include applications of nonlinear optics, optical signal processing for communication systems, and fiber lasers. She has authored more than 100 publications in international peer-reviewed journals and conferences.

Govind P. Agrawal is currently the James C. Wyant Professor at the Institute of Optics of the University of Rochester. He is an author or coauthor of eight books and more than 450 research articles. He is a fellow of the Optical Society (OSA) and a life fellow of IEEE. He was the editor-in-chief of OSA's *Journal Advances in Optics and Photonics* during 2014–2019. He was the recipient of IEEE Quantum Electronics Award in 2012, the Esther Hoffman Beller Medal in 2015, the OSA Max Born Award in 2019, and the EPS Quantum Electronics and Optics Medal in 2019.